Millimeter-wave Liquid Crystal Polymer Based Antenna Array for Conformal 5G Applications

Syeda Fizzah Jilani, *Student Member, IEEE*, Max Munoz, *Member, IEEE*, Qammer H. Abbasi, *Senior Member, IEEE*, and Akram Alomainy, *Senior Member, IEEE*

***Abstract*—This paper presents the design, fabrication and performance evaluation of a flexible millimeter-wave (mm-wave) antenna array for the fifth generation (5G) wireless networks operating at K_a-band (26.5–40 GHz). The single element antenna is comprised of a tapered rectangular patch with a coplanar-waveguide (CPW) feed. The ground is designed with L-shaped stubs to converge the dispersed radiation pattern for improving the directivity and gain. The antenna fabrication is accomplished by two highly precise methods of laser-milling and inkjet printing on a flexible liquid crystal polymer (LCP) substrate. Moreover, a novel method of time-efficient sintering is also introduced. The design is further extended in a two-element array for the gain enhancement. Measurements have validated that the antenna array exhibits a bandwidth of 26-40 GHz with a peak gain of 11 dBi at 35 GHz, and consistent high gain profile of above 9 dBi in the complete K_a-band. These potential features recommend the proposed antenna array as an efficient solution for integration in future flexible 5G front-ends and mm-wave wearable devices.**

***Index Terms*—5G, flexible, inkjet, LCP, wireless.**

I. Introduction

FLEXIBLE and conformal antennas are highly anticipated for mm-wave based 5G architecture in many applications such as airborne, vehicular, cellular as well as body-centric devices to facilitate a compact, robust and reliable integration of wireless technology [1]. 5G is envisioned to establish a versatile, diverse, ultra-dense, and unified network with the advantages of device miniaturization, conformal implements, low profile and cost-effective fabrication. Recently, precise and low-cost manufacturing techniques such as inkjet printing, screen printing and laser prototyping, have greatly augmented the realization of antennas on the flexible substrates [2, 3]. Several low-frequency flexible antennas have been developed and more intense efforts are in progress at mm-wave spectrum to advance towards the conformal implements for 5G. Various synthetic and organic materials such as, polymers, polyesters and textiles have been used for the antenna design [4, 5]. LCP is regarded as attractive for high-frequency flexible antennas due to its low dielectric constant of 2.9 ~ 3.1, low loss-tangent of 0.002 at mm-wave frequencies, lower moisture absorption, resistant to chemicals, and capable to withstand temperatures up to 300˚C [6, 7]. In addition, mechanical flexibility, low coefficient of thermal expansion, and availability in a range of thicknesses (25–180 μm), suggest that LCP is a suitable choice for implementing mm-wave conformal antennas [8].

The high bandwidth demands of an efficient, diverse, and seamless 5G communication could only be accomplished by using mm-waves [9]. Choice of a suitable frequency band with minimal attenuations and propagation losses is of great interest to the regularity authorities. Among the available mm-wave bandwidth, K_a-band is highlighted for 5G due to lower absorptions, lesser path loss, and reduced signal fading [10, 11]. The US Federal Communications Commission (FCC) has recommended 28- and 38-GHz bands for 5G standards, while Ofcom UK has developed 5G testbeds on 26-GHz [12]. These variants have aggravated a need of a high-bandwidth antenna for 5G front-ends, which can simultaneously support multiple standards, and ensures a reliable performance in terms of high gain and efficiency over the operating range. Also, the antenna should be compact, low profile, less-complex, and conformal. In this paper, a K_a-band LCP based antenna is designed to address the 5G demands, and fabricated by two state-of-the-art methods of laser prototyping and inkjet printing for the comparative performance analysis. Moreover, heat sintering of the inkjet-printed prototype is usually time-consuming, which has been improved in this work by using a heat press instead of the oven to efficiently reduce the sintering duration from several minutes to just a few seconds. The antenna design is extended further in an antenna array for the gain enhancement.

II. Design Methodology and Fabrication

Finite Integration Technique (FIT) based CST STUDIO SUITE is used for the modeling and numerical evaluation. Flexible film of Rogers ULTRALAM 3850 LCP is selected as a substrate. The mm-wave monopole antenna is comprised of a tapered rectangular patch with a CPW feed, and a pair of stubs integrated with the ground. The length of the patch is tapered to increase the radiating length. L-shaped stubs are placed on either side of the patch at a specified distance. This particular ground structure is capable to suppress the radiation of a conventional omnidirectional monopole antenna along the horizontal axis and converges its radiation orthogonal to the

Manuscript received July 7, 2018;

S. F. Jilani is with the School of Electronic Engineering and Computer Science, Queen Mary University of London, London E1 4NS, U.K., and also with the National University of Sciences and Technology, Islamabad, Pakistan (e-mail: s.f.jilani@qmul.ac.uk).

Qammer H. Abbasi is with University of Glasgow., Glasgow G12 8QQ, U.K. (e-mail: Qammer.Abbasi@glasgow.ac.uk)

Max Munoz and A. Alomainy are with the School of Electronic Engineering and Computer Science, Queen Mary University of London, London E1 4NS, U.K. (e-mail: a.alomainy@qmul.ac.uk).

antenna plane. Parametric analysis of the design parameters, for instance, the size and geometry of the stubs and distance between the stub and patch, is important to achieve desired characteristics. Fig. 1 (a) shows a CST model of the proposed antenna along with the parameters, while the corresponding dimensions are illustrated in Table I. In order to inspect the antenna performance in conformal positions, CST model of the antenna is bent along the curved surface of a cylinder of radius 10 mm, as shown in Fig. 1 (b). *K*-connector is also modeled for close estimations of actual measurements. Fig. 1 (c) shows that the design is extended further into an array of the tapered patches. CPW feed is designed with two additional small stubs placed in close proximity of the feeding network for appropriate coupling in order to attain suitable impedance matching. The distance between the patch centers is set as λ/2 of the lower resonant band, i.e. 28 GHz to avoid coupling. The stubs' length in the antenna array is parametrically increased to enhance the directivity. Parametric analysis is carried out for the suitable positioning of stubs. The antenna array is also bent to perform conformal analysis as shown in Fig. 1 (d).

The antenna of dimensions 11 × 12 mm^2 is fabricated on Rogers ULTRALAM 3850 with the thickness (h) = 100 μm, dielectric constant (ε_r) = 2.9, and loss tangent (tanδ) = 0.0025. Two fast and precise fabrication processes, i.e. LPKF laser milling and inkjet printing are suggested for the comparative analysis and resultant prototypes are presented in Fig. 1 (e), while the array is fabricated with laser prototyping as shown in Fig. 1 (f). LCP films are typically available with a surface metal cladding for subtractive techniques of prototyping [13]. Protolaser-U4 machine is deployed, which utilizes laser beam to etch off the copper layer of thickness 17.5 μm in a precise pattern with a high resolution of up to 15 μm. However, in the second process, the cladding is fully removed by a chemical treatment with ferric chloride ($FeCl_3$) solution (molar mass = 270.3 g/mol) and then clear LCP is rinsed with distilled water. The LCP film is then subjected to the additive technique of flatbed inkjet printing in the Dimatix materials printer (DMP-2831) with drop spacing of 15 μm (i.e., 1693.33 dpi), firing voltage of 15 V, and jetting frequency of 5 KHz.

The quality and conductivity of the inkjet-printed pattern are determined by the ink composition. For instance, high ink viscosity due to a larger proportion of nanoparticles yields better conductivity, though results in a compromise on print quality as viscosity affects the seamless jetting of the ink from the printhead nozzles. The conductive ink (i.e., Colloidal Ag-J solid Ag) consists of 20.3% of solid silver content is selected. Silver nanoparticles are encapsulated with monolayer polymer to avoid oxidation and suspended in an inert solvent. Sintering process is essential to break the protective polymer sheath and combines the particles for better continuity. The conductivity of the printed layer is typically 0.4 ~ 2.5 × 10^7 S/m, based on a number of successive iterations, layer thickness, temperature, and time intervals involved in curing and sintering processes.

The proposed antenna is inkjet-printed as a 0.5 μm thin silver pattern with a resolution of ±20 μm on a LCP substrate. The granular nature of silver layer with irregular bulges and lumps due to particle coalescence is observed in Fig. 2 (a), which shows that the nanoparticles remain captured in the polymer after drying, which aggravates a need of sintering process. Sintering uses high-energy exposure either by a laser source or an elevated temperature treatment, to break the sheath and combines the molten ink particles for continuity. Several methods have been proposed which involve high-energy laser beams or ovens [13, 14]. Heat sintering takes a long time and requires several minutes or even hours for high-temperature curing, which may cause wrinkling, shrinking or decolorization to the substrate. For instance, one method suggests curing for 40 minutes at 180 ˚C in an oven [13]. Similarly, much higher risk of damage of printed pattern or substrate is involved with laser sources if the intensity and exposure time is not controlled [14]. LCP depicts an excellent temperature handling profile but prolong heating durations have been avoided in this work by proposing a novel method. The printed prototype is dried in an oven for 5 minutes to evaporate the ink solvent and then a heat press with a pre-set temperature of 160˚C is used for 30 seconds duration. The prototype is placed between Kapton films and protective Teflon sheets during the exposure time to avoid direct contact

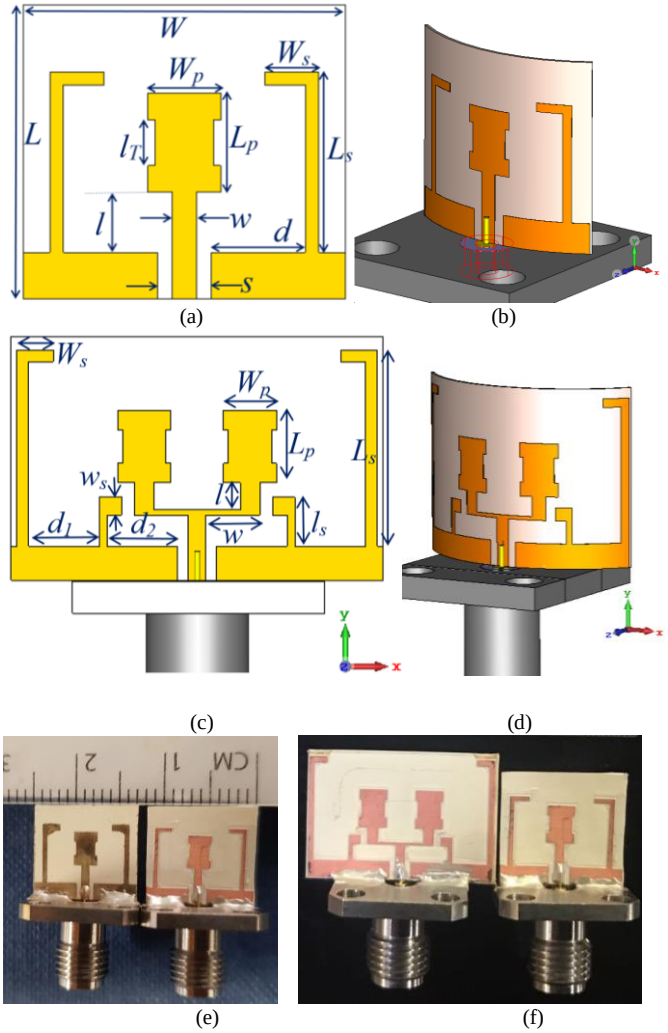

Fig. 1. Proposed flexible frequency-reconfigurable two-element MIMO antenna: (a) simulated antenna model; (b) inkjet-printed fabricated prototype; (c) conformal MIMO antenna.

of press plates with the print. This new method is anticipated as highly time-efficient among all the reported heat sintering processes and offers good conductivity of 0.3×10^7 S/m with no damage to the substrate or printed pattern. Fig. 2 (b) shows that bulges and surface irregularities have disappeared as the neighboring particles combine together in the sintered pattern.

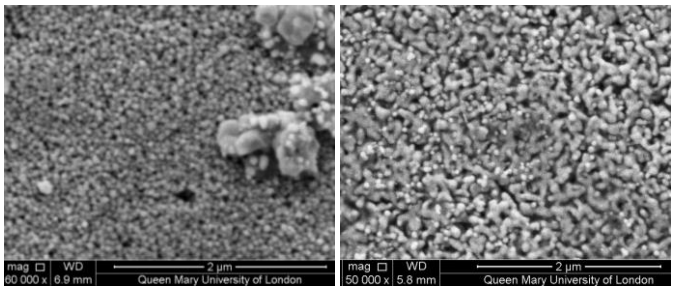

(a) (b)

Fig. 2. SEM images of the inkjet-printed silver nanoparticle layer: (a) layer particles before sintering, (b) layer particles after sintering.

TABLE I. DIMENSIONS OF THE PROPOSED SINGLE PATCH ANTENNA

Parameters	mm	Parameters	mm
Length of patch, L_p	3.7	Feed width, w	0.9
Width of patch, W_p	2.7	Feed length from edge, l	2.25
Ground stub length, L_s	6.75	Tapered length, l_T	1.7
Ground stub width, W_s	2	CPW gap, s	2
Antenna length, L	11	Edge-to-stub distance, d	3.5
Antenna width, W	12		

TABLE II. DIMENSIONS OF THE PROPOSED PATCH ANTENNA ARRAY

Parameters	mm	Parameters	mm
Length of patch, L_p	3.7	Feed width, w	2.75
Width of patch, W_p	2.7	Feed length, l	1.4
Stub 1 length, L_s	10.05	Stub 2 length, l_s	2.5
Stub 1 width, W_s	1.85	Stub 2 width, w_s	0.9
Gap of two stubs, d_1	3.6	Stub 2 distance, d_2	3.6

III. NUMERICAL AND EXPERIMENTAL ANALYSES

Experimental results of *S*-parameters, radiation pattern, and realized gain demonstrate that the measurements are in good agreement with the simulations, though some differences exist mainly due to the connector or cable losses.

A. Impedance Bandwidth

Fig. 3 (a) compares reflection coefficient (S_{11}) plots of the proposed antenna fabricated by two different processes; i.e. laser milling and inkjet printing. The measured results of both antennas depict similar profile though the resonating band of inkjet-printed antenna is shifted to some extent. The intended bandwidth of K_a-band in fairly conserved in both cases. Fig. 3 (b) presents the measurements taken in different scenarios of in-air, on fabric and on-body of the laser prototyped antenna, which shows its reliable performance in wearables. Fig.3 (c) shows a close match between the simulated and measured results of the antenna and array. Conformity analysis in Fig. 3 (d) depicts that the bandwidth remains conserved even if the prototypes of antenna and array are folded or bended.

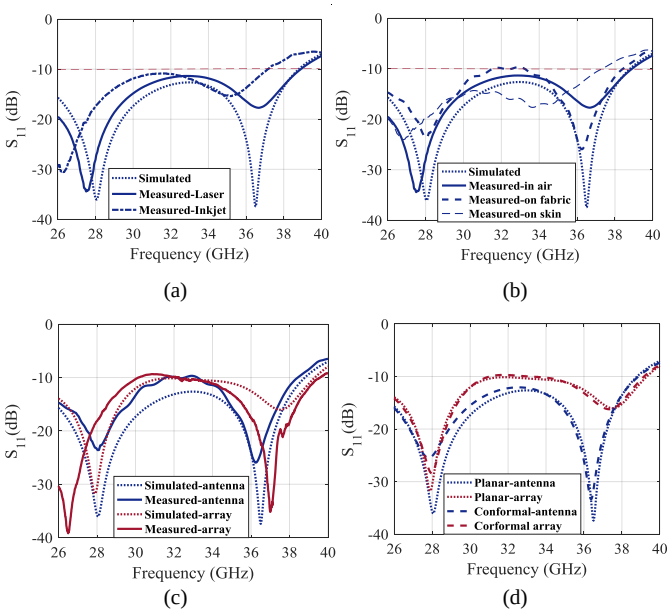

Fig. 3. S_{11} plots of the flexible mm-wave antenna: (a) single antenna S_{11} with both methods of fabrication, (b) laser prototyped antenna measured in air, on fabric and on human skin, (c) S_{11} of single antenna and 2-element array, (d) simulated results of conformal antenna and array.

B. Radiation Pattern

The radiation patterns of the flexible mm-wave antenna exhibit an evenly distributed pattern on the front and back, with maximum directivity titled to some extent from the axis orthogonal to the antenna surface. The two-element antenna array also shows similar profile as of single antenna, though the main beam is further shifted from the $\theta = 0^\circ$. Fig. 4 shows the simulated and measured results with dashed and bold lines respectively, of the designed antenna and two-element array configuration, at $\varphi = 0^\circ$ and $\varphi = 90^\circ$ on distinct frequencies of the K_a-band. The $\varphi = 0^\circ$ plots show the expected radiation suppression alone the horizontal axis due to designed stub geometry. While $\varphi = 90^\circ$ plots depict that the main beam is tilted from the perpendicular axis where the big metal size of connector could be partially responsible for this tilt.

C. Realized Gain

The consistent gain profile is extremely essential in the complete bandwidth to deliver a reliable antenna response. Usually, the gain doesn't always remains same in the complete operating range and may vary in the wide operating bandwidth of monopole patch antennas. This discrepancy often restricts the use of certain frequencies of a high impedance bandwidth due to relatively lesser and insufficient gain performance. One of the distinctive features of the proposed antenna is its fairly consistent realized gain profile and direction of maximum radiation in the overall bandwidth, which suggests its reliable performance throughout the proposed range of operation. The simulated and measured results of the realized gain of mm-wave antenna and array topology against the frequency has been presented in Fig. 5. Two antenna gain method is utilized for gain calculations and the results show similar findings as that of the computational evaluations. Numerically estimated efficiency profile of Fig. 5 also shows that the antenna is highly efficient in the operating range of the K_a-band.

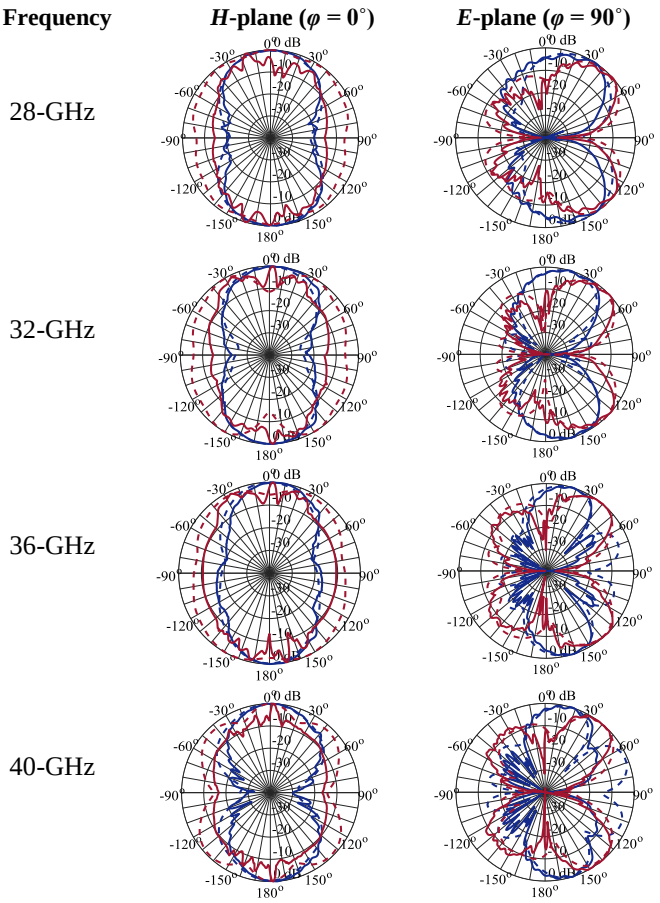

Fig. 4. Simulated (dashed line) and measured (bold line) normalized radiation patterns of the flexible mm-wave antenna (in Blue) and array (in Red).

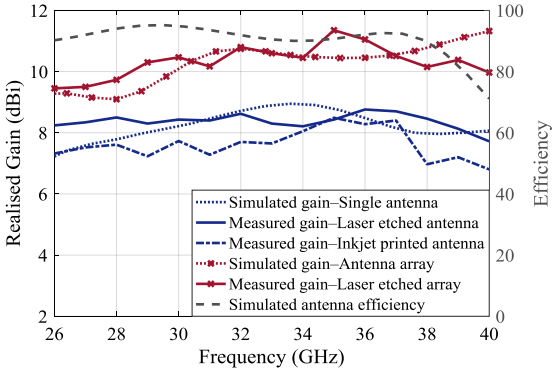

Fig. 5. Simulated and measured realized gain plots of the flexible mm-wave antenna and array as well as the simulated antenna efficiency.

Comparison of the presented work with the recent antennas designed on the frequencies of interest is provided in Table III. It is observed that the designed antenna array dominates due to the combined advantages of high gain, wide bandwidth, conformity, and better scan area with two radiating beams.

TABLE III. COMPARISON OF PROPOSED WORK WITH RECENT ANTENNAS

	Bandwidth (GHz)	Gain (dBi)	Flexible	Radiation
[4]	22–40	4.2–8.2	✓	omnidirectional
[14]	34–35.8	10–12	✓	Single beam
[15]	26.9–30.6	6.0–8.0	×	Single beam
[16]	Ant-1: 27.7–30	10–12.1	×	Single beam
	Ant-2: 27.2–28.7	6.8–7.4	×	
Proposed	Ant: 26–40	8.0–8.76	✓	Two beams
work	Array: 26–40	9.5–11.35	✓	

IV. CONCLUSION

This paper has presented a low-profile, mm-wave antenna design and its array topology for the potential deployment in 5G conformal applications. The design is comprised of a CPW-fed tapered rectangular patch and a symmetrical pair of L-shaped stubs as a part of ground. The proposed antenna has been fabricated by two advanced methods on a flexible LCP substrate, and a novel and time-efficient sintering technique has been introduced. The antenna covers a bandwidth of 26–40 GHz with a measured peak gain of 8.76 dBi at 36 GHz, with the gain above 8 dBi in the complete range. Moreover, the proposed two-element array retains the bandwidth of K_a-band with the enhanced gain of 11.35 dBi at 35 GHz, while the gain is above 9 dBi in the overall range. The mm-wave flexible antenna array is highly suitable for 5G wearables and combines the high gain and high bandwidth profiles with the ease of fast and precise fabrication techniques.

REFERENCES

[1] H. A. Elmobarak Elobaid *et al.* "A transparent and flexible polymer-fabric tissue UWB antenna for future wireless networks," *IEEE Antennas Wireless Propag. Lett.*, vol. 16, pp. 1333–1336, 2017.

[2] D. Godlinski *et al.*, "Printing technologies for the manufacturing of passive microwave components: antennas," *IET Microw. Antennas Propag.* , vol. 11, no. 14, pp. 2010–2015, 2017.

[3] M. Y. Chen *et al.*, "Conformal ink-jet printed *C*-band phased-array antenna incorporating carbon nanotube field-effect transistor based reconfigurable true-time delay lines," *IEEE Trans. Microw. Theory Tech.*, vol. 60, no. 1, pp. 179–184, 2012.

[4] S. F. Jilani and A. Alomainy, "Planar millimeter-wave antenna on low-cost flexible PET substrate for 5G applications," *10th European Conf. Antennas Propag. (EuCAP)*, 2016, pp. 1–3.

[5] H. R. Khaleel *et al.*, "A compact polyimide-based UWB antenna for flexible electronics," *IEEE Antennas Wireless Propag. Lett.*, vol. 11, pp. 564–567, 2012.

[6] H. L. Kao *et al.*, "Bending effect of an inkjet-printed series-fed two-dipole antenna on a liquid crystal polymer substrate," *IEEE Antennas Wireless Propag. Lett.*, vol. 13, pp. 1172–1175, 2014.

[7] G. DeJean *et al.*, "Liquid crystal polymer (LCP): a new organic material for the development of multilayer dual-frequency/dual-polarization flexible antenna arrays," *IEEE Antennas Wireless Propag. Lett.*, vol. 4, pp. 22–26, 2005.

[8] N. Altunyurt *et al.*, "Conformal antennas on liquid crystalline polymer based rigid-flex substrates integrated with the front-end module," *IEEE Trans. Adv. Packag.*, vol. 32, no. 4, pp. 797–808, 2009.

[9] D. Liu *et al.*, "What will 5G antennas and propagation be?" *IEEE Trans. Antennas Propag.*, vol. 65, no. 12, pp. 6205–6212, 2017.

[10] T. S. Rappaport *et al.*, "Overview of millimeter wave communications for fifth-generation (5G) wireless networks—with a focus on propagation models," *IEEE Trans. Antennas Propag.*, vol. 65, no. 12, pp. 6213–6230, 2017.

[11] W. Hong, K. H. Baek and S. Ko, "Millimeter-wave 5G antennas for smartphones: Overview and experimental demonstration," IEEE Trans. Antennas Propag., vol. 65, no. 12, pp. 6250–6261, 2017.

[12] W. Hong, "Solving the 5G mobile antenna puzzle: Assessing future directions for the 5G mobile antenna paradigm shift," *IEEE Microw. Mag.*, vol. 18, no. 7, pp. 86–102, 2017.

[13] E. Tekin *et al.*, Direct synthesis and inkjetting of silver nanocrystals toward printed electronics Adv. Funct. Mater., 2007, 17, 277

[14] Y. J. Cheng *et al.*, "Millimeter-wave shaped-beam substrate integrated conformal array antenna," *IEEE Trans. Antennas Propag.*, vol. 61, no. 9, pp. 4558–4566, 2013.

[15] S. Alkaraki *et al.*, "Compact and low cost 3D-printed antennas metalized using spray-coating technology for 5G mm-wave communication systems," *IEEE Antennas Wireless Propag. Lett.*, 2018.

[16] J. S. Park *et al.*, "A tilted combined beam antenna for 5G communications using a 28-GHz band," *IEEE Antennas Wireless Propag. Lett.*, vol. 15, pp. 1685–1688, 2016.